13th Int Symp on Applications of Laser techniques to Fluid Mechanics
Lisbon, Portugal, 26-29 June, 2006
#1354

Stereoscopic PIV Analysis of an Oscillating Piezoelectric Unimorph

Simon J.Croucher[1], Nicholas J.Lawson[1], Kranti K. Lal Kummari[2], Hsien-Chun Chung[2], Zhaorong Huang[2] & Roger Whatmore[3]

1: School of Engineering, Cranfield University, Cranfield, UK
s.j.croucher@cranfield.ac.uk, n.lawson@cranfield.ac.uk
2: Department of Materials, Cranfield University, Cranfield, UK,
k.k.lalkummari@cranfield.ac.uk, h.chung.2003@cranfield.ac.uk
z.huang@cranfield.ac.uk
3: Tyndall National Institute, Cork, Ireland. roger.whatmore@tyndall.ie

ABSTRACT

Interest in flapping flight has significantly increased in recent years as a possible platform for novel micro air vehicle (MAV) designs. Piezoelectric fans have found use as an actuation system for such applications in addition to cooling fan applications for use within high power electronic devices.

In this investigation the resonant frequency was obtained by means of varying the applied frequency to a piezoelectric unimorph between 5Hz and 50 Hz, while at a constant sinusoidal applied voltage of 150V. This was found to be 30 Hz. While at the resonant frequency, the applied voltage was then varied, from 60V to 150V, in order to vary the tip amplitude from 5.2mm to 11.8mm and both instantaneous and time averaged 3-D stereoscopic PIV images of the flow field were obtained and analysed to provide both the magnitude and direction of the surrounding flow.

The system was based on dual Photron APX cameras and a New Wave Pegasus Nd:YLF laser with TSI Insight 3G software. The seeding system used was a Martin Magnum 800.

At the lower range of tip amplitudes tested (Reynolds number 356 and 1314), the relatively large tip amplitude produces a vertical jet acting towards the tip of the unimorph with an associated system of counter rotating vortices. However, a transition of the flow regime at the larger tip amplitude (Reynolds number 1777) occurs and produces a vertical jet acting predominantly away from the tip of the unimorph. For all cases tested, the vortex system is found to be off-axis and may occur as a result of the initial conditions of the experiment. The centreline velocity profiles confirm transition in the flow regime as the amplitude, and hence Reynolds number, increases. Instantaneous vector plots and point velocity profile throughout a cycle outlines the periodic nature of the flow.

1. Introduction.

The interest in flapping flight as a platform for micro air vehicles (MAV's) has significantly grown in recent years (McMichael and Francis, 1997; Woods et al., 2001; Ellington, 1999). As a method of actuation, the use of piezoelectric lead zirconate titanate (PZT) materials may be used (Sitti et al., 2001). Additional applications include cooling fans within high power electronic applications (Toda, 1979, 1980; Yoo et al., 2000; Wu and Ro, 2005). Being very compact with low electromagnetic noise while having a long lifetime and low power consumption make the use of piezoelectric materials in either application extremely promising.

The simplest design, a unimorph, consists of a patch of piezoelectric ceramic material bonded to a thin elastic metal cantilever shim (see figure 1) and acts as a composite electromechanical structure converting electrical input into mechanical strain. An alternating voltage applied across the

thickness of the material causes the device to oscillate as a result of a bending deformation generated within the piezoelectric ceramic.

In the context of cooling applications, flow visualisation studies of small amplitude oscillating piezoelectric fans have provided quantitative results (Ihara and Watanabe, 1994; Acikalin et al., 2004b; Burmann et al., 2003). Numerical simulations (Acikalin, 2002) and PIV analysis (Kim et al., 2004) have provided a more detailed quantitative analysis of the complex flow field. Two major components of the structure were apparent. Counter rotating vortices were shed at the point of maximum deflection. This affected the spanwise flow while also influencing the flowfield downstream where a jet-like flow was observed from the fan tip, as modelled by Acikalin et al. (2003).

Similar vortical signatures and jet-like flow has been in the wakes of pitching aerofoils (Freymuth, 1988; Triantafyllou et al., 1993; Koochesfahani, 1989). However, there is a key difference between the flow field of the two cases where the latter is subject to a nominal freestream velocity whereas the former case in normally located within a static flow field.

While significant work has been completed on small amplitude oscillating fans, there is limited flow data for a large amplitude tip deflection. Thus, this investigation will use stereoscopic PIV to provide both qualitative and quantitative 3-D data for the flow field surrounding an oscillating piezoelectric fan for a range of both frequencies and amplitudes.

2. Experimental Method and Procedures.

2.1 Piezoelectric Unimorph

The unimorph consisted of a stainless steel metal shim and one piezoelectric patch made of commercially available PSI-5H4E, as outlined in figure 1. The patch was mounted such that a length of the metal shim was free to vibrate. The glue used to bond the two together was assumed to have negligible thickness. The fan was fixed in a cantilevered manner, with one end clamped and one end free. Care was taken when clamping as this had a significant effect on the dynamics and performance of the fan. As a result, the length of the fan extending beyond the clamp was 41mm with an effective fan length, l_o, of 29.7mm (Toda, 1979).

The unimorph was then located within a glass enclosure made of 3mm thick glass of internal dimensions 200mm x 200mm x 400mm (based upon the unimorph coordinate system, figure 2) and fixed in place using clear sealant. This was done so as to regulate initial conditions. A signal generator and amplifier were used to vary the sinusoidal voltage and frequency. Applied voltage was varied from zero to a maximum value which varied the tip amplitude. Only positive values were used to ensure the unimorph was driven in the correct manner.

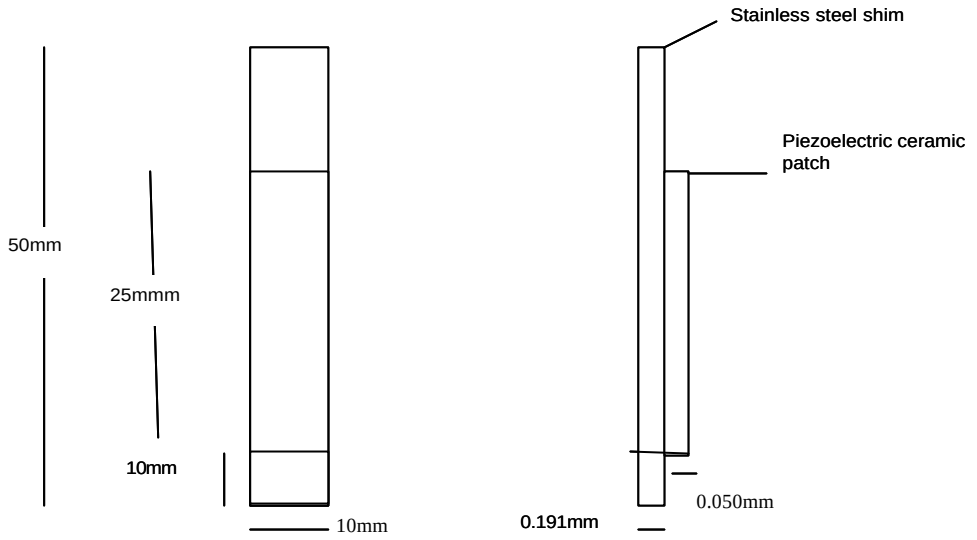

Figure 1. Details of the pie zoelectric unimorph

2.2 Stereoscopic PIV

Figure 2 outlines the stereoscopic imaging system used to record the flow fields. A New Wave Pegasus Nd:YLF double pulsed laser, of wavelength 527nm and pulse energy of 10mJ per pulse, was used with a combination of lenses to create a 2mm thick light sheet aligned with the vertical centre plane of the fan. Images were acquired using two, 2MP Photron APX CCD cameras with a resolution of 1024 x 1024 pixels and 256 grey scale colour. Located in the forward scatter mode either side of the light sheet at 45º, camera separation and object distances were fixed at 226mm and 320mm respectively, resulting in a symmetric set-up. Micro Nikon lenses with focal lengths 60mm (f4.0) were used to obtain an area of interest of 80mm x 80mm with a mean resolution of 78µm per pixel. System control and image analysis was provided by TSI Insight v7.2.2 commercial PIV software.

Seeding for the system was supplied using a Martin Magnum 800 fog generator. The seeding was added to the enclosure and allowed to both mix and settle for approximately one minute before images were taken. A light box was also placed before the front of the enclosure to limit the laser sheet to just above the tip of the fan so as to minimise the heating of the piezoelectric material. This conduction was found to induce a convection flow from earlier tests.

One hundred image pairs were used to produce mean flow and first order statistics. The number of images used was based upon a compromise between flow accuracy and computation time and also the analysis proposed by Kim et al. (2004). A total of 8 complete cycles could be analysed at the resonant frequency based upon a laser repetition frequency of 250Hz and ?t of 2000µs. Image analysis was completed using a multi-pass adaptive window shifting Recursive Nyquist grid engine (32X32 -16x16 pixels) with a FFT correlator and Gaussian peak engine. A simple validation technique based upon pixel range was used to erase erroneous vectors caused by uncoupled particle pairs. Tecplot v10 was used to produce the vector maps for each case.

Calibration of the system was a two stage process. Initially, a 10 x 10 calibration grid with 10mm spacing was placed in the centre of the light sheet/object plane to allow alignment of the cameras with the grid to ensure both cameras imaged a common object plane. Images of the grid were then obtained. 3-D reconstruction was then completed using the calibration software within Insight to produce calibration coefficients that were used to de-warp the images. Given a full scale displacement equivalent to around 5 pixels, a camera half angle of 45° and assuming a typical

measurement error of 0.1 pixel (Westerweel, 1997), will lead to an error ration of one and in-plane and out-of-plane full scale errors of 2% (Lawson and Wu 1997).

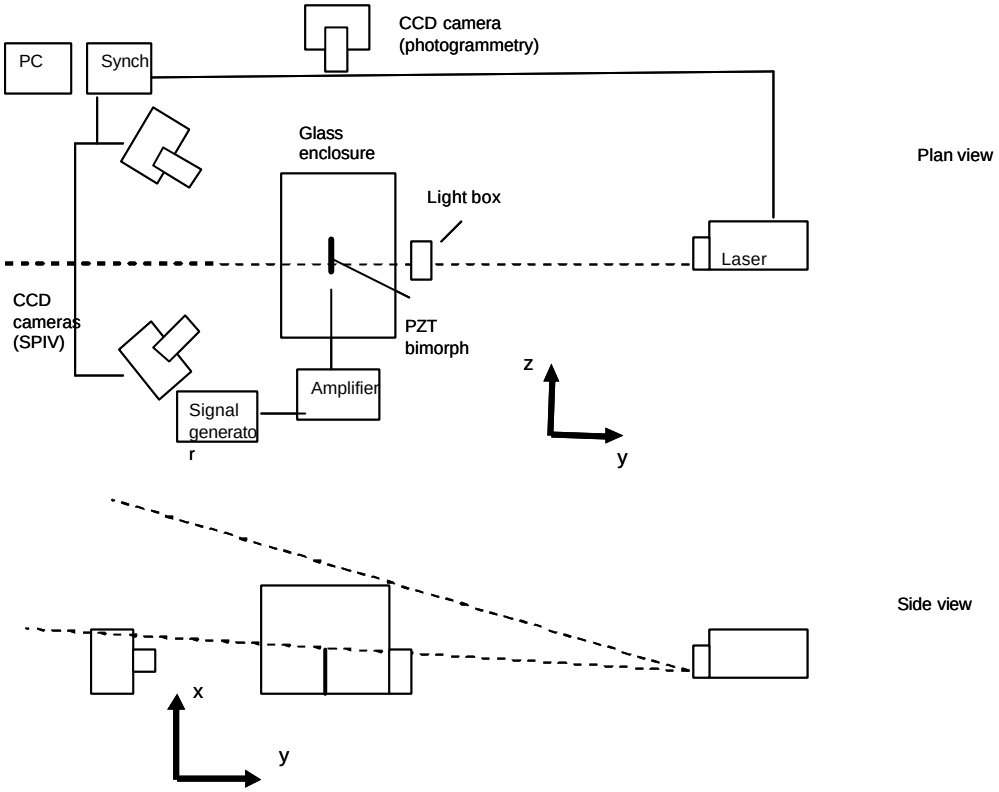

Figure 2. Schematic of the experimental set-up

2.3 PZT Tip Displacement

Using the same laser system as for the stereoscopic PIV analysis, a single 2MP Photron APX camera, orientated perpendicular to both the light sheet and plane of the fan oscillation, was used to measure the tip deflection for numerous frequency/applied voltage combinations. Fitted with a 60mm (f2.8) Nikon lens and the same resolution, an area of interest of 51.25mm x 51.25mm corresponded to a mean resolution of 50µm per pixel. As previously, TSI Insight v7.2.2 was used to control the timing of the system. Based upon the limitations of the cameras, the time separation was kept constant at 1000µs with a corresponding laser frequency of 500Hz. A light box was used to ensure only the tip of the fan was illuminated to ease the analysis. One hundred images were taken resulting in up to a total of 16 complete cycles being analysed at the resonant frequency

Analysis of the data was completed manually using commercially available software. Each image was assessed and tip coordinates were evaluated based upon the coordinates of the pixels with the highest intensity at the tip.

3. Results and Discussion.

3.1 Tip Deflection

A sinusoidal applied voltage was assumed and initially, the resonant frequency was analysed. At the maximum applied voltage setting, frequency was varied and the tip amplitude was evaluated. Figure 3 shows the expected relationship between frequency and tip amplitude where the first mode resonant frequency is clearly visible, occurring at 30Hz.

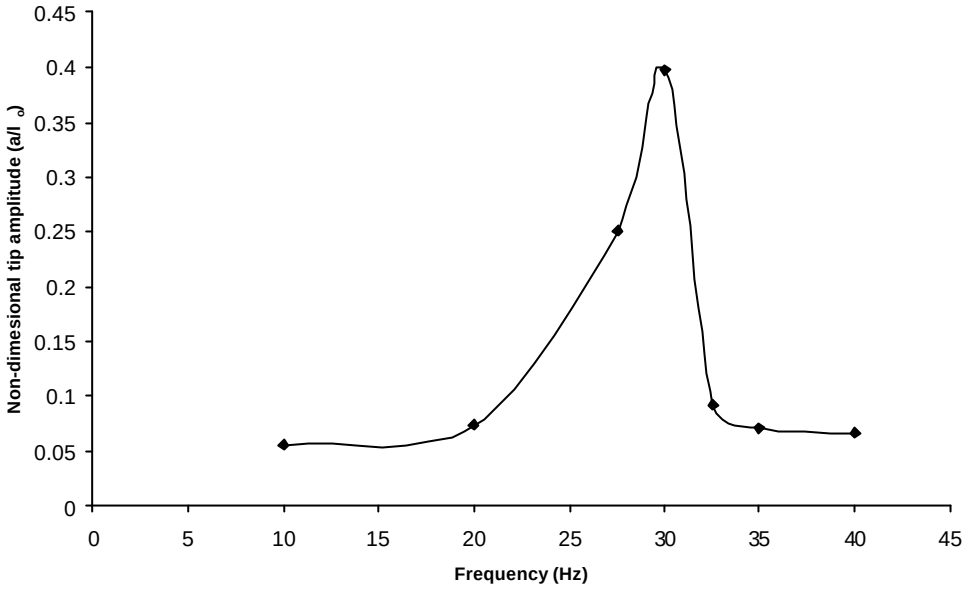

Figure 3. Tip amplitude deviation with varying frequency at largest applied voltage (150V)

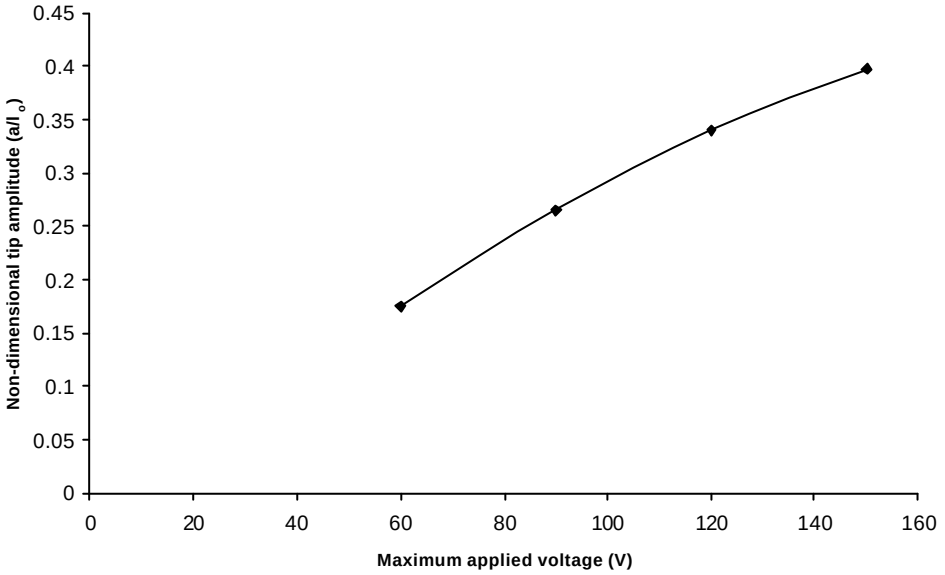

Figure 4. Variation of tip amplitude with applied voltage at resonant frequency (30Hz)

The relationship between tip amplitude and applied voltage variation was also analysed for the unimorph when oscillating at its resonant frequency, figure 4. This is shown to be a linear relationship, as expected. However, based upon a least squares best fit line, a non-zero intersect is apparent at zero volts. Both hysteresis and a non-zero minimum voltage would both result in voltage, and hence force, being present in the unimorph which would change the minimum tip amplitude and hence total amplitude. The maximum non-zero voltage, given as a percentage of the maximum voltage, was found to be 1.9%. Hysteresis effects were not investigated.

Reynolds number based upon the total tip amplitude and tip velocity, with tip velocity V_T = ?a = 2? f_oa and Reynolds number $Re_a = V_T a/?$ (given resonant frequency, f_o and tip amplitude, a). In this instance 3 cases were investigated with Re = 1777, 1314 and 356 with corresponding non-dimensional tip amplitudes a/l_o= 0.397, 0.340 and 0.176. Compared to previous investigations (Kim

et al., 2004) tip amplitude is an order of magnitude larger resulting in a significantly larger Reynolds range, although tip velocity is of a similar range. In addition Strouhal number, St = $f_o a/V_T$ used to define the growth of a well defined series of vortices as found in pitching/plunging/flapping motion, was found to be constant, St=0.16.

3.2 Velocity Measurement.

3.2.1 Time Averaged PIV

A similar flow field composition to that observed at the lower tip amplitudes is observed with the two major flow components present; a counter rotating vortical structure in addition to a jet like flow. However, the specific details in each case are very different, particularly at the lower range of amplitudes tested. Time averaged 3-D plots, figures 5, 6 & 7, outline the complex flow field for the three cases investigated.

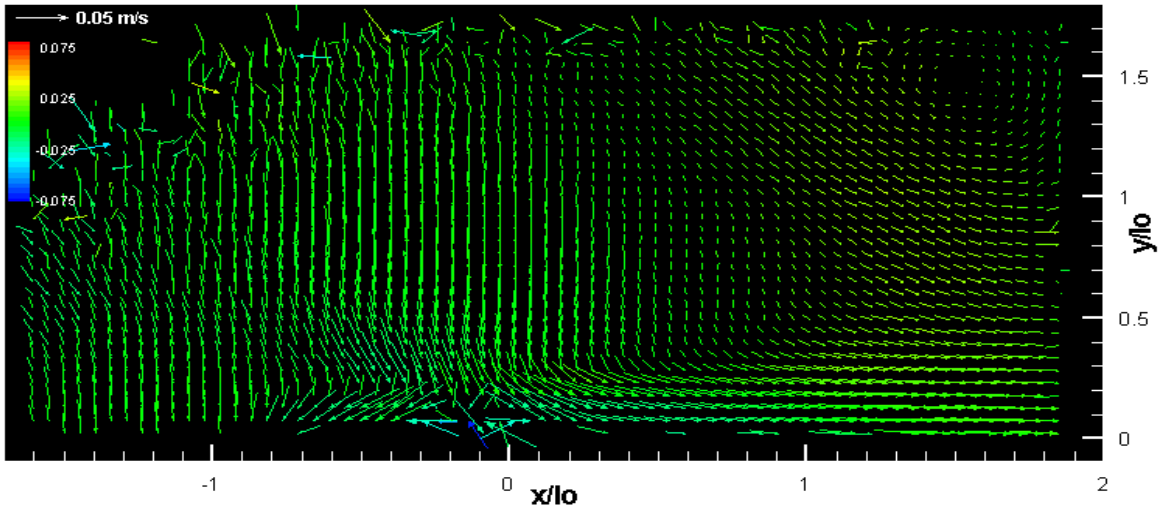

Figure 5. Time averaged vector plot for a/l_o = 0.176, Re_a = 356

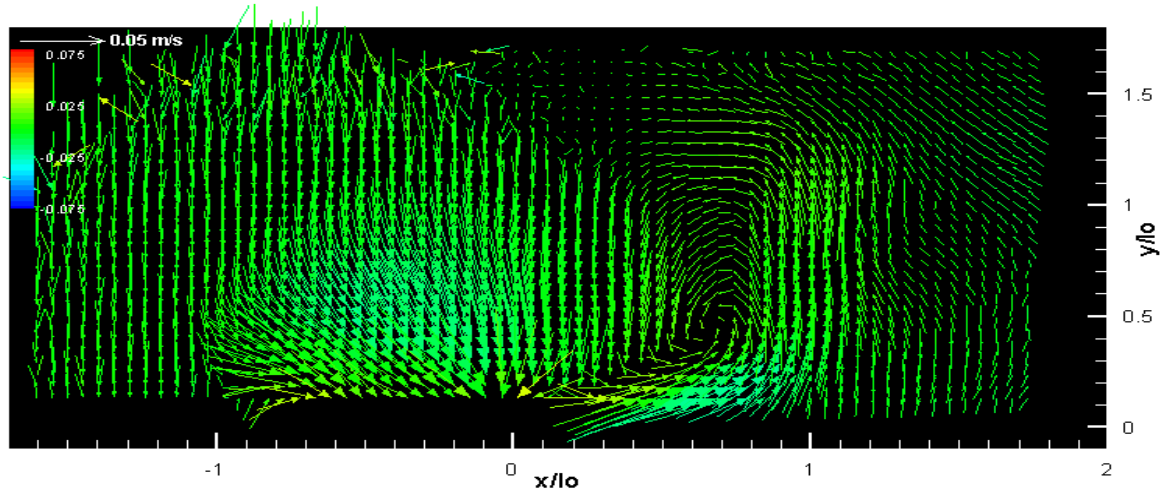

Figure 6. Time averaged vector plot for a/l_o = 0.340, Re_a = 1314

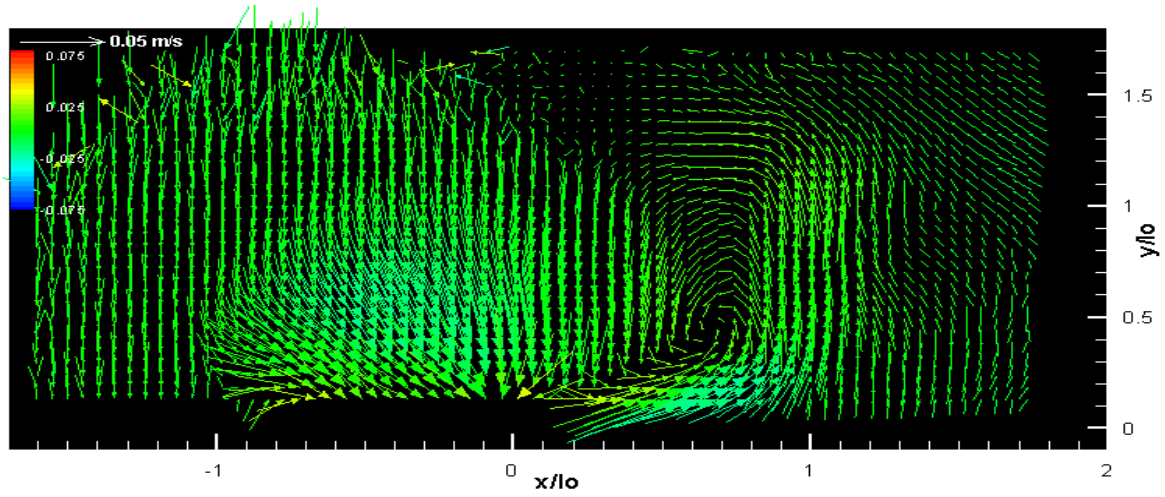

Figure 7. Time averaged vector plot for $a/l_o = 0.396$, $Re_a = 1777$

The flow field structure shows a downward induced jet-like flow towards the tip, located at (0,0) in the images, most apparent in figure 5, at $Re_a = 356$, in addition to shed counter rotating vortices. The magnitude of the tip amplitude is such that the pressure distribution results in a large suction area causing the downward jet-like flow.

Although a region of downward jet-like flow is seen near the tip of the fan at the largest amplitude tested ($a/l_o = 0.397$, $Re_a = 1777$), an upward jet is also seen suggesting a shift in the flow regime. For either scenario, the jet flow has significant influence on the surrounding flow field which extends far beyond the amplitude of the fan characteristic dimension. This flow structure has been previously reported (Ihara and Watanabe, 1994; Kim et al., 2004) and is found mostly on the left hand side of the image, closer to the front of the box.

With regards to the vortex pattern, although tow counter-rotating vortices are generated, the vortex pattern is found to be asymmetric with a larger vortex apparent on the right hand side of the images which corresponds to the rear of the box. The circulation associated with the vortex pattern is consistent with the direction of the jet-flow.

As the amplitude increases so too does the strength of both the jet-flow and vortices. At $a/l_o = 0.176$ ($Re_a = 356$), the jet-flow structure is predominantly vertical with a velocity of around 0.023m/s (or around 2.3% of the tip velocity). Upon reaching the tip the flow is turned and becomes almost horizontal travelling away from the tip eventually resulting in a shed vortex downstream from the tip. This is apparent in the top right hand corner of the image. Its strength is relatively small as indicated by vectors being both small in magnitude with a significant jet divergence angle of the order 45º. For $a/l_o = 0.340$ ($Re_a = 1314$), the jet flow is found to increase in magnitude having a peak velocity of around 0.036m/s (but only 1.9% of the tip velocity). Vortex strength is also found to increase significantly, as indicated by the magnitude and closeness of the vectors. Finally at $a/l_o = 0.397$ ($Re_a = 1314$), significant circulation is present in the region close to the tip, creating the downward jet region, and in the far field associated with the upward jet. Thus, it may be suggested that the complexity and influence of the boundary conditions generated by the box increases as the amplitude of the oscillation increases. A significant point to note that the jet velocity is two orders of magnitude lower than the tip velocity contradicting previous investigations which suggested the

jet velocity may be as much as two to four times the tip velocity (Ihara and Watanabe, 1994; Kim et al., 2004).

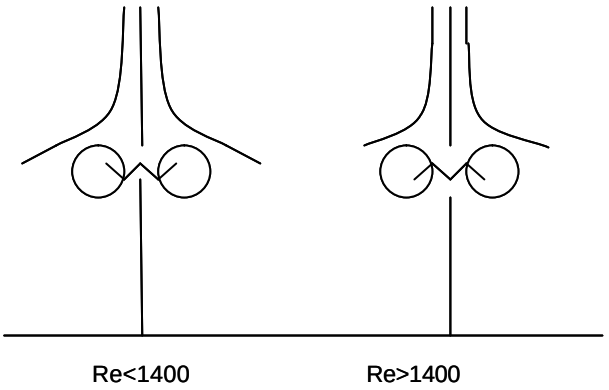

Figure 8. Schematic of the proposed flow regime variation

The general flow structure and variation in the structure may be described by figure 8 which indicates a schematic of the flow field. For either regime, two counter rotating vortices are shed per cycle inducing a vertical jet-like flow. In the case of the two lower amplitudes (Re_a = 356 and 1314), as the fan oscillates from right to left a clockwise vortex is shed at the point of maximum deflection while a counter clockwise vortex is shed as the tip moves from left to right. The rotation of the vortices, caused by the suction effect of the oscillation, is such that the resultant jet-like flow acts downward towards the tip of the fan. As the regime changes so too does the sense of the vortex circulation. As the tip moves from left to right to the point of maximum deflection, a counter clockwise vortex is shed with a corresponding clockwise vortex shed as the tip moves from right to left. The resultant jet-like flow is induced upwards.

Confirmation of the change in the flow regime is given by figure 9 which shows the centreline velocity distribution for the three cases, where positive velocity U is downward. For the lower two amplitudes a similar distribution is seen where the velocity decreases, in magnitude, with distance from the tip of the fan as would be expected. The distribution itself is similar in shape to that observed previously (Kim et al., 2004). Although no data is available at the tip itself, it may be inferred that the maximum velocity, equivalent to the tip velocity, is found in this region. It should be noted that the velocity is always positive indicating a downward jet. Comparing the two, for a/l_o = 0.340 (Re_a = 1314) a jet is apparent further downstream of the tip than for a/l_o = 0.176 (Re_a = 356) indicating the greater influence the former has on the surrounding fluid. For a/l_o = 0.397 (Re_a = 1777) a significant difference is apparent. The jet is found to be positive in direction and hence acting downward near the tip but changes to a negative direction or an upward acting jet downstream reaching a peak at around y/l_o =0.4 before decreasing once again as distance increases. It should also be noted that although the initial jet is smaller in magnitude than the other two cases, the secondary upward acting jet is of comparable magnitude to that a/l_o = 0.176 (Re_a = 356). The jet is apparent further downstream indicating the greatest influence upon the surrounding fluid. The very different two velocity profiles confirm the change in flow regime.
Comparisons with previous work have found a limited amount of data is available at such low Reynolds numbers. Numerous studies have investigated the aerodynamics and associated forces for both fixed and flapping wings suitable for micro air vehicle flight. However, the majority of this data is still at Reynolds numbers at least an order of magnitude larger than the present study. Kunz and Kroo (2001) investigated the aerodynamics at very low Reynolds number for fixed wing aerofoils. Data obtained at Re = 1000 shows a change in the lift curve slope from the linear relationship followed by a rapid stall as expected at higher Reynolds numbers to a less linear

increase followed by a more gradual stall. As the Reynolds number decreases, the effect of viscosity dominates and the development of the boundary layer is of prime importance. Once again, little is known about the development of boundary layers at such low Reynolds numbers. Thus, it is clear that a transition occurs between conventional high Reynolds number flow and low Reynolds number flow as investigated here.

A large asymmetry in the flow field is seen and may occur as a result of small initial disturbance within the experimental area of interest. An unstable average flow is found for a pitching aerofoil (Anderson et al., 1998) with the unstable flow being inclined if the oscillating speed is greater that the freestream velocity (Jones et al., 1998). Ultimately, the condition acts as a narrow band amplifier with the ability to randomly switch its inclination under conditions of flow disturbance. In the absence of any flow disturbances the inclination of the flow is determined by the by the initial conditions, such as laser misalignment or a slightly asymmetric fan deflection. Given that all three cases were under the same experimental conditions, this seems a likely explanation.

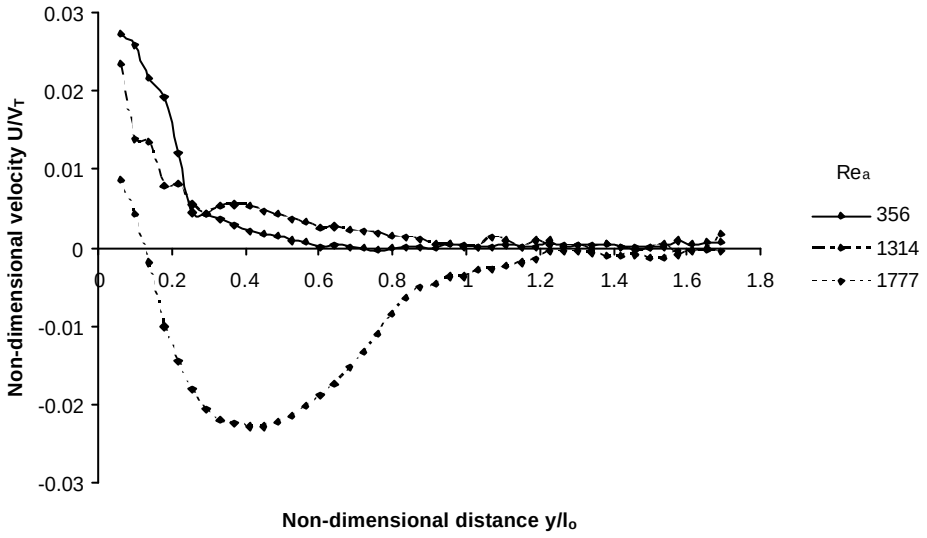

Figure 9. Centreline velocity distribution for the three amplitudes

3.2.2 Instantaneous PIV

Figure 10 shows a sequence of instantaneous images for $a/l_o = 0.397$ ($Re_a = 1777$) indicating the development of the flow. The major point of note is around the tip where the flow is found to increase both in strength and rotation before shedding of the vortex occurs. Over this small time step, the flow around the tip is found to vary significantly whereas the general flow field varies very little. In this time instance, the maximum velocity can be clearly seen downstream of the tip but slightly off axis. It is assumed that throughout the entire cycle, a similar pattern is found on the other side of the fan resulting in a symmetric jet. Two vortices are seen on the right hand side of the image with one developing in the top right hand corner and one developing just to the right of the region of maximum velocity. The periodic nature of the flow may be seen as a result. This is confirmed by the velocity variation for a given point over 2 complete cycles, figure 11, and clearly shows that the variation is indeed sinusoidal, as would be expected.

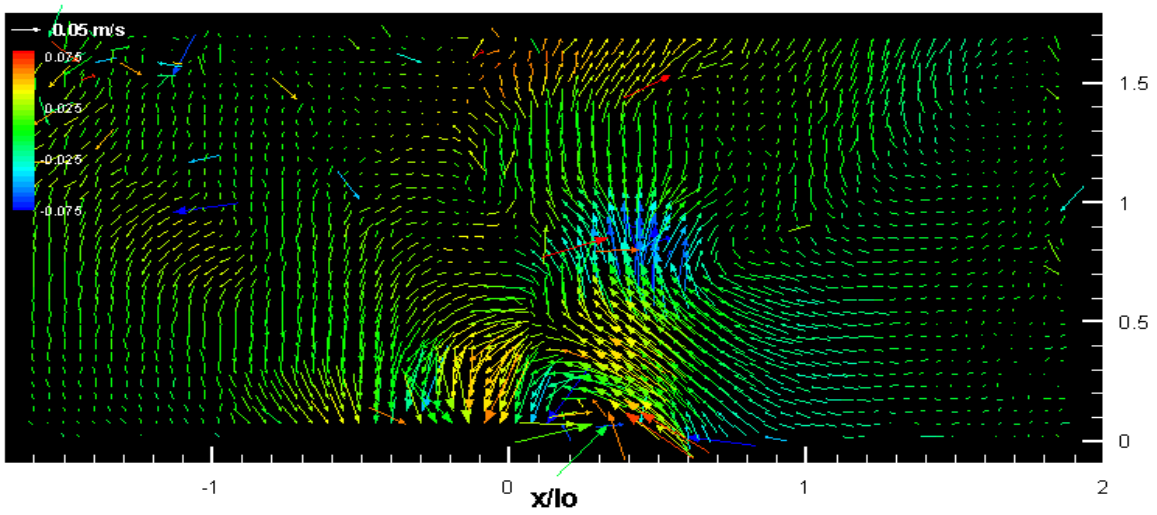

Figure 10a. Instantaneous vector plot for $a/l_o = 0.397$ ($Re_a = 0.1777$)

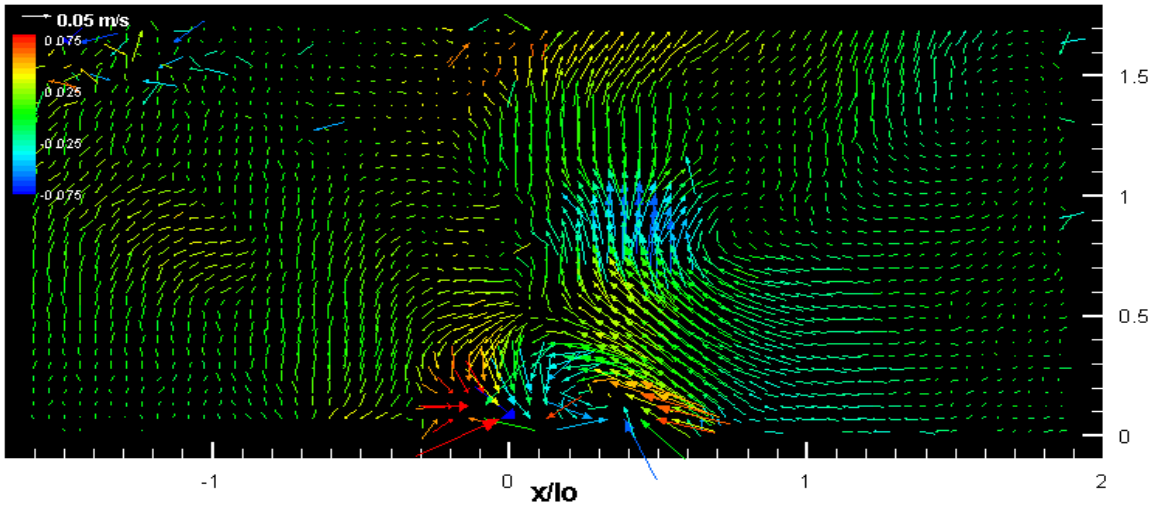

Figure 10b Instantaneous vector plot for $a/l_o = 0.397$ ($Re_a = 0.1777$)

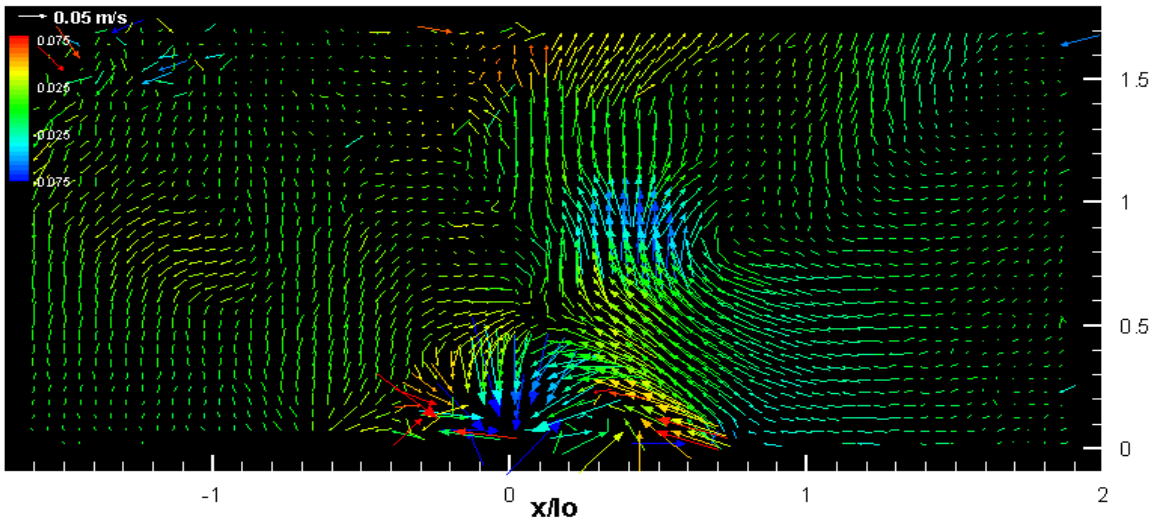

Figure 10b Instantaneous vector plot for $a/l_o = 0.397$ ($Re_a = 0.1777$)

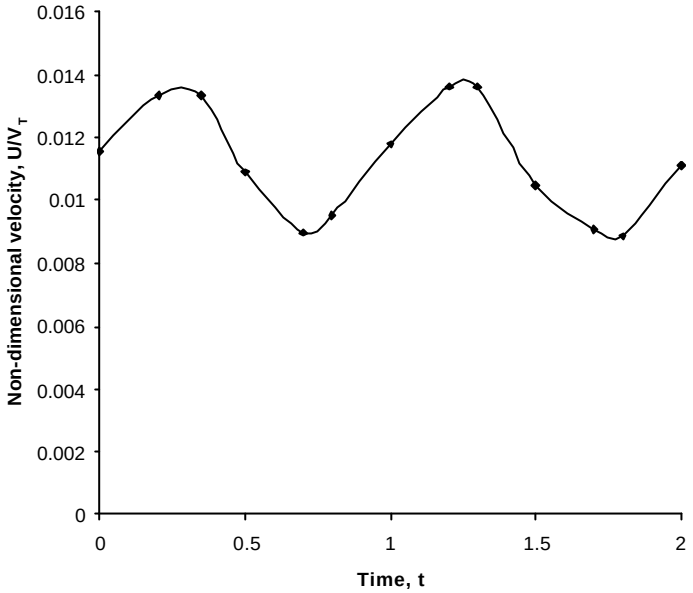

Figure 11. Velocity variation for a given point throughout the oscillation

4. Conclusions.

This investigation has used stereoscopic PIV techniques to investigate the flow field associated with large amplitude oscillations of a piezoelectric fan operating at its first resonance. Tip deflection measurements follow the expectedrelationship for variation in both applied voltage and applied frequency. Time resolved vector plots are found to indicate a highly complex flow with a downward acting jet for the lower amplitudes (Re_a = 356 and 1314) while a flow regime variation at the larger amplitude (Re_a = 1777) results in an upward acting jet. Instantaneous vector plots indicate the development and periodic nature of the flow throughout a cycle.

Further investigation is required into the transition of the flow regime as tip amplitude, and hence Reynolds number, increases as limited previous data is currently available for these types of flow.

References

Açikalin, T. (2002). “Numerical Simulation of Fluid Flow Generated by Piezoelectric Fans Vibrating in its First Mode”, MSc Thesis, Prudue University, IN, USA, pp 1-8.

Açikalin, T., Raman, A. and Garimella, S.V. (2003). “ Two-Dimensional Streaming Flows Induced by Resonating Thin Beams”, Journal of Acoustical Society in America, 114, pp 1785-1795.

Açikalin, T., Wait, S.M., Garimella, S.V. and Raman, A. (2004b). “Experimental Investigation of the Thermal Performance of Piezoelectric Fans”, heat Transfer Engineering, 25, pp 4-14.

Adrain, R.J. (1991). “Particle Imaging Techniques for Experimental Fluid Mechanics”. Annual Review of Fluid Mechanics, 23, pp 261 – 304.

Anderson, J.M., Streitlien, K., Barrett, D.S. & Triantafyllou, M.S. (1998). “Oscillating Foils of High Propulsive Efficiency”. Journal of Fluid Mechanics 360, pp 41

Bürmann, P., Raman, A. and Garimella, S.V. (2003). “Dynamics and Topology Optimisation of Piezoelectric Fans”, IEEE Transactions on Components and Packaging Technologies, 25, pp 592-600

Ellington, C.P. (1999). “The Novel Aerodynamics of Insect Flight: Applications to Micro Air Vehicles”, Journal of Experimental Biology 202, pp 3439-3448.

Freymuth, P. (1988). "Propulsive Vortical Signatures of Plunging and Pitching Airfoils". AIAA Journal 26, pp 881 – 883.

Hinsch, K.D.(1993). "Particle Image Velocimetry". Speckle Metrology. 38, 235-324. 1993. New York, Marcel Decker Inc.

Hinsch, K. D. (1995). " Three-dimensional Particle Image Velocimetry". Measurement Science and Technology 6, pp 742-753.

Ihara, A. and Watanabe, H. (1994). "On the Flow Around Flexible Plates Oscillating with Large Amplitudes", Journal of Fluids and Structures, 8, pp 601-619.

Jones, K.D., Dohring, C.M. & Platzer, M.F. (1998). "Experimental and Computational Investigation of the Knoller-Betz Effect". AIAA Journal 36, pp 1240

Kim, Y-H., Wereley, S.T. and Chun, C-H. (2004). "Phase-Resolved Flow Field Produced by a Vibrating Cantilever Plate Between Two Endplates", Physics of Fluids, 16, pp 145-162.

Koochesfahani, M.M. (1989). "Vortical Structures in the Wake of an Oscillating Airfoil". AIAA Journal 27, pp 1200 – 1205.

Kunz, P.J. & Kroo, I. (2001). "Analysis and Design of Airfoils for Use at Ultra-Low Reynolds Numbers", Fixed and Flapping Wing Aerodynamics for Micro Air Vehicle, Ed Muller, T.J.

Lawson, N.J. & Wu, J. (1997). "Three-dimensional Particle Image Velocimetry: Error Analysis of Stereoscopic Techniques". Measurement Science and Technology 8, pp 894 – 900.

McMichael, J.M. and Francis, M.S. (1997) "Micro Air Vehicles - Towards a New Dimension in Flight", www.euler.aero.iitb.ac.in/docs/ MAV/www.darpa.mil/tto/MAV/mav_auvsi.html

Prasad, A K. (2000). "Stereoscopic Particle Image Velocimetry". Experiments in Fluids 29, pp 103-116.

Raffel, M., Willert, C. and Kompenhans, J. (1998). " Particle Image Velocimetry: A practical guide". Springer.

Toda, M. (1979). "Theory of Air Flow Generation by a Resonant Type PVF_2 Bimorph Cantilever Vibrator", Ferroelectrics, 22, pp. 911-918.

Toda, M. (1981). "Voltage-Induced Large Amplitude Bending Device – PVF_2 Bimorph- Its Properties and Applications", Ferroelctrics, 32, pp. 127-133.

Triantafyllou, G.S., Triantafyllou, M.S. and Grosenbaugh, M.A. (1993). "Optimal Thrust Development in Oscillating Foils with Application to Fish Propulsion", Journal Of Fluids and Structures 7, pp 205 – 224.

Westerweel, J. (199). "Fundamentals of Digital Particle Image Velocimetry", Measurement Science and Technology, 8, pp 1379 - 1392

Woods, M.I., Henderson, J.F., and Lock, G.D. (2001). "Energy Requirements for The Flight of Micro Air Vehicles", Aeronautical Journal 105, pp 135-149.

Wu, T. and Ro, P.I. (2005). "Heat Transfer Performance of a Cooling System Using Vibrating Piezoelectric Beams", Journal of Micromechanics and Microengineering, 15, pp 213-220.

Yoo, J.H., Hong, J.I. and Cao, W. (2000). "Piezoelectric Ceramic Bimorph Coupled to Thin Metal Plate as Cooling Fan for Electronic Devices", Sensors and Actuators, 79, pp 8-12.